Effects of Li and Y co-doping on electrical properties and dielectric relaxation behavior of BCZT ceramics

Chang-Qun Wang[1], Chun Shu[1], De-Yi Zheng[1,*] (ID), and Shun Luo[1]

[1] *College of Materials and Metallurgy, Guizhou University, Guiyang 550025, Guizhou, China*

ABSTRACT

In order to research the effects of Li and Y (Li/Y) co-doping on BCZT ceramics, lead-free $(Ba_{0.85}Ca_{0.15})$ $(Ti_{0.9}Zr_{0.1})$ + xLi$_2$CO$_3$ + xY$_2$O$_3$ (abbreviated as BCZT-Li$_x$Y$_x$, x = 0, 0.1, 0.2, 0.3, and 0.4 mol%) piezoceramics were synthesized by traditional solid-state sintering method. The phase structure and microstructure of ceramic samples were researched through XRD and SEM. The electrical properties of ceramic samples were researched by piezoelectric, dielectric, and ferroelectric test instruments. The XRD spectrums indicate that ceramic samples have the perovskite structure. The SEM images show that the introduction of Li/Y in BCZT ceramics can promote grain growth and densification. The temperature-dependent dielectric performance testing results prove that BCZT-Li$_x$Y$_x$ ceramic samples have apparent dielectric relaxation behavior. Moreover, co-doping Li/Y in BCZT ceramics can effectively decrease the sintering temperature from 1540 °C to 1400 °C and improve the electrical properties. The optimal electrical properties are obtained at x = 0.3 mol% (d_{33} = 526 pC/N, k_p = 58%, ε_r = 4724, tanδ = 0.017, T_c = 75.5 °C, γ = 1.63, P_r = 9.73 μC/cm^2, E_c = 2.10 kV/cm).

1 Introduction

Pb(Zr$_{1-x}$Ti$_x$)O$_3$ (PZT)-based ceramics with excellent piezoelectric properties are widely used in various electronic materials, including actuators, sensors, and transducers. However, the lead is easy to volatilize at high temperature, which will endanger human beings and the environment [1–6]. Over the past years, lead-free piezoelectric materials such as K$_{0.5}$Na$_{0.5}$NbO$_3$ (KNN)-, Bi$_{0.5}$Na$_{0.5}$TiO$_3$ (BNT)-, and BaTiO$_3$ (BT)-based ceramics have become research hotspots [7, 8]. Among these lead-free ceramics, BT-based ceramics have attracted widespread attention due to their relatively high piezoelectric coefficient (d_{33} ~ 190pN/C) and electromechanical coupling coefficient [8].

Recently, Liu and Ren [9] discovered that Ba(Zr$_{0.2}$Ti$_{0.8}$)O$_3$-(Ba$_{0.7}$Ca$_{0.3}$)TiO$_3$ (BCZT) ceramics by introducing Zr^{4+} and Ti^{4+} into BT-based ceramics possessed high piezoelectric properties (d_{33} = 620 pC/N). The excellent piezoelectric property could be attributed to the coexistence of rhombohedral and tetragonal phases around the tricritical triple point. However, the sintering temperature of BCZT

ceramics is high (1540 °C) [10]. Hence, many researchers begin to utilize the method of doping modification to reduce the sintering temperature of BCZT ceramics.

In terms of doping modification, metal oxides such as Li_2CO_3 [11–13] and CuO [14, 15] are often used as sintering aid and introduced into BCZT ceramics to reduce the sintering temperature. Zhang et al. [11] found that the appropriate introduction of Li_2CO_3 into BCZT ceramics can reduce the sintering temperature by 100–150 °C due to the emergence of oxygen vacancies and the liquid phase. But its electrical properties (d_{33} = 340 pC/N, k_p = 44%) need further improvement. Chen et al. [12] reported that adding 0.3 wt% Li_2CO_3 into BCZT ceramics can lower sintering temperature from 1540 °C to 1450 °C and maintain the piezoelectric properties at 512 pC/N. However, the electromechanical coupling coefficient (k_p = 49%) is still at a low level. From the above discussion, it can be found that adding Li_2CO_3 into BCZT ceramics can effectively reduce the sintering temperature, but the electrical properties are not significantly improved. Many studies [16, 17] show that rare earth oxide Y_2O_3 can effectively enhance the electrical properties of BCZT ceramics. Mittal et al. [16] reported that by introducing 0.02 mol% Y_2O_3 into BCZT ceramics, the piezoelectric coefficient, electromechanical coupling coefficient, and remanent polarization are increased by approximately 70%, 18%, and 47%, respectively.

In this work, Li_2CO_3 and Y_2O_3 were co-doped into BCZT ceramics for reducing their sintering temperature and improving their electrical properties. BCZT-Li_xY_x piezoceramics were synthesized through traditional solid-state sintering method. Meanwhile, the effects of Li/Y co-doping on phase structure, microstructure, electrical properties, and dielectric relaxation behavior of BCZT ceramics were systematically analyzed.

2 Experimental procedures

The $(Ba_{0.85}Ca_{0.15})(Ti_{0.9}Zr_{0.1})$ + xLi_2CO_3 + xY_2O_3 (abbreviated as BCZT-Li_xY_x, x = 0, 0.1, 0.2, 0.3, and 0.4 mol%) lead-free piezoceramics were synthesized by traditional solid-state sintering method. The chemicals including $BaCO_3$ (99.9%), $CaCO_3$ (99.9%), TiO_2 (99.8%), ZrO_2 (99.8%), Li_2CO_3 (98%), and Y_2O_3 (99.9%) were used as raw materials. First, these oxide powders were weighed according to the stoichiometric proportion of the BCZT-Li_xY_x composition. Then, these oxide powders were ball-milled in alcohol for 24 h and were dried for 8 h. The mixed powders were calcined at 1200 °C for 2 h. After calcination, the powders were ball-milled in alcohol for 20 h again and were dried for 8 h again. The powders were granulated with 5 wt% paraffin as a binder. Then, the powders were pressed into tablets with a diameter of 12 mm and a thickness of 1.2 mm under 30 MPa. Finally, the ceramic samples were separately sintered at 1380 °C, 1400 °C, 1420 °C for 4 h and the electrical properties are optimal at 1400 °C.

The phase structure of ceramic samples was characterized by X-ray diffraction (XRD, Model Panalytical/X'pert-PRO, Holland). The microstructure of ceramic samples was obtained by field emission scanning electron microscopy (FE-SEM, Model SUPRA40, Germany). To test electrical properties, the ceramic samples were sintered at 700 °C for 30 min after coating the silver pastes on both surfaces. Then, the ceramic samples were polarized in the silicone oil bath at 25 °C under a direct current electrical field of 3.0 kV/mm for 30 min. After laying the polarized ceramic samples for 24 h to release remnant stress and charge, the piezoelectric coefficient (d_{33}) was measured by a quasi-static d_{33} meter (Model ZJ-3AN, Chain). The electromechanical coupling coefficient (k_p) at 1 kHz was calculated by using an electron oscillator (Model UX21) resonance and anti-resonance technique. Before calculating the dielectric constant (ε_r) at room temperature, dielectric loss ($\tan\delta$) and capacitance (C) were measured by using a capacitance tester (Model TH2618B). The dielectric constant as a function of temperature was measured with an impedance analyzer (Model WK6500B, UK). Besides, the measured temperature range was from 20 °C to 250 °C and frequencies were 100 Hz, 1 kHz, 10 kHz, 100 kHz, and 1 MHz. The ferroelectric hysteresis loops (P–E) of ceramic samples were measured by a Radiant Precision Premier LC ferroelectric tester (Radiant Technologies Inc, Albuquerque, NM) at 3 kV, 10 Hz, and room temperature.

3 Result and discussion

3.1 Phase structure of ceramic samples

Figure 1 presents the XRD spectrums of BCZT-Li_xY_x ceramic samples. As shown in Fig. 1a, the diffraction peaks of all ceramic samples correspond to the diffraction peaks of perovskite structure (ABO_3), and there are no obvious stray peaks. This indicates that ceramic samples have the perovskite structure. To further analyze the effects of Li/Y co-doping on phase structure of BCZT ceramics, the magnified XRD spectrums in the range of 44.6°–46° are shown in Fig. 1b. It is worth noting that the diffraction peaks first shift to lower angles and then to higher angles with the addition of Li/Y, which means that the doping of Li/Y in BCZT ceramics can induce lattice distortion. According to the principle of tolerance factor and Bragg's law ($2d\sin\theta = \lambda$), where A-site is occupied by large ions [$r(R^{3+}) > 0.094$ nm] and B-site is occupied by small ions [$r(R^{3+}) < 0.0087$ nm]. The ionic radii of Ba^{2+}, Ca^{2+}, Zr^{4+}, Ti^{4+}, Li^+, and Y^{3+} are 0.138 nm, 0.106 nm, 0.072 nm, 0.060 nm, 0.076 nm, and 0.090 nm, respectively. Therefore, Li^+ can occupy B-site and the crystal lattice is slightly expanded owing to the similar radius of Li^+ (0.076 nm) and Zr^{4+} (0.072 nm). Y^+ is an amphoteric dopant and can occupy both A-site and B-site. Y^{3+} occupying A-site or B-site is the main cause of lattice distortion due to the large radius difference between Y^{3+} and host elements. It was reported [17] that Y^{3+} first replaces B-site and then replaces A-site after B-site is saturated. When $x = 0.1$ mol%, the content of Li^+ could not saturate B-site. Thus, Y^{3+} will also occupy B-site. This situation will cause crystal lattice expansion and increase interplanar crystal spacing. In contrast to the radius effect, Y^{3+} and Li^+ occupying B-site will produce oxygen vacancies because of the occurring of acceptor doping, which decreases interplanar crystal spacing. Wu et al. [17] found that the radius effect is more significant than the oxygen vacancy effect on shifting peaks. Thus, the diffraction peaks shift to lower angles. When $x > 0.1$ mol%, the content of Li^+ could be able to saturate B-site. Therefore, Y^{3+} would enter A-site, which will lead to lattice shrinkage and decrease interplanar crystal spacing. Further, Li^+ entering B-site will produce oxygen vacancies owing to the occurring acceptor dopant, which decreases interplanar crystal spacing. Y^{3+} entering A-site will break the balance of charge distribution owing to the occurring of donor doping and decrease the interplanar distance. Thus, the diffraction peaks reversely shift to higher angles.

Moreover, it can be seen from Fig. 1b that the diffraction peaks are composed of multiple peaks, which indicates the coexistence of multiphase in these ceramic samples [18]. Figure 2 shows the Rietveld XRD spectrums and Rietveld refinement parameters of BCZT-Li_xY_x ceramic samples at $x = 0$ mol% and $x = 0.3$ mol%. The phase structure of the ceramic samples changes from orthogonal and tetragonal (O–T) phases coexistence to rhombohedral and tetragonal (R–T) phases coexistence after adding 0.3 mol% Li/Y to BCZT ceramics. Yang et al. reported [19] that in BZT-xBCT system, when the composition moves to C_2 that approaches the R–O boundary from the R side, O phase develops into a metastable state. In addition, at composition C_2, the

Fig. 1 XRD spectrums of BCZT-Li_xY_x ceramic samples. **a** $2\theta = 20°–80°$ **b** magnified XRD spectrums in the range of 44.6°–46°
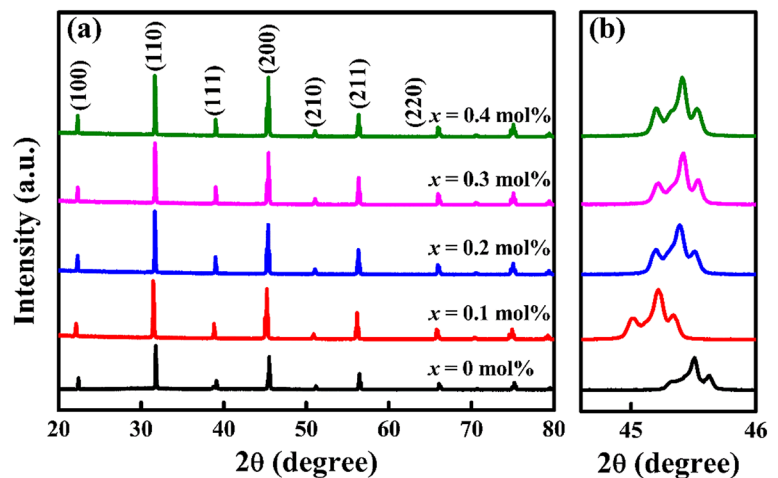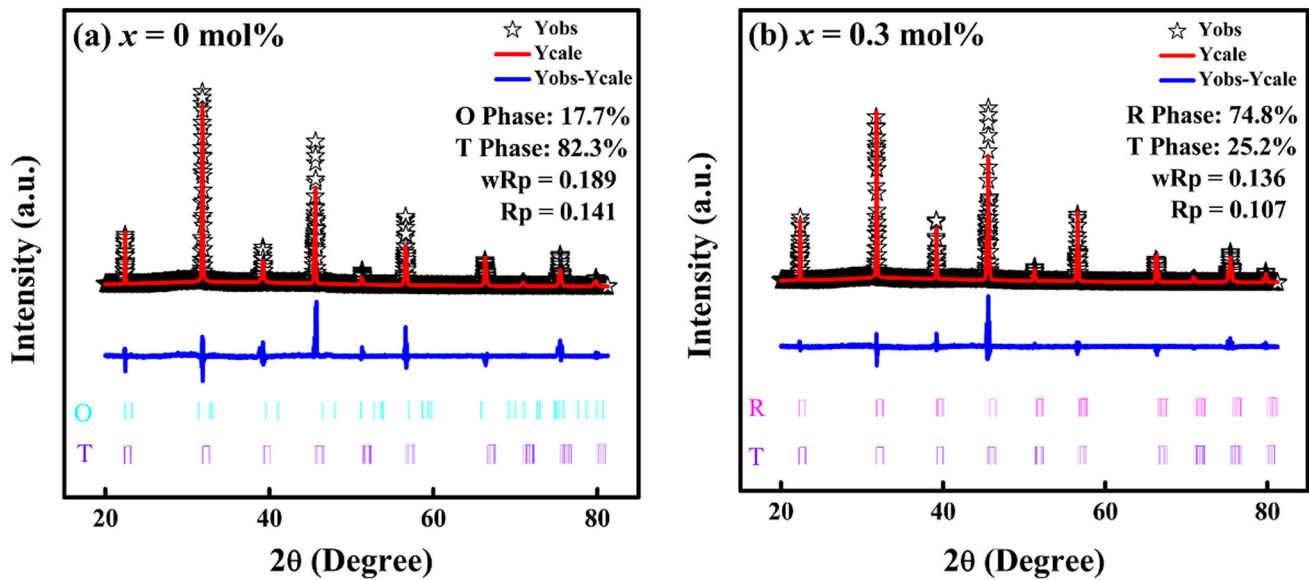
Fig. 2 Rietveld XRD spectrums and Rietveld refinement parameters of BCZT-Li$_x$Y$_x$ ceramic samples

activation energy required for the transformation of the stable R phase to the metastable O phase is equal to the energy barrier for direct domain switching between two R variants. But the activation energy needed for the transition from the metastable O phase to the stable R phase is even smaller than the energy barrier for direct domain switching between two R variants. Therefore, after adding 0.3 mol% Li/Y to BCZT ceramics, the energy barrier required for the transformation from O phase to R phase is low, resulting in the coexistence of R–T phases. The coexistence of R–T phases in BCZT ceramics has also been reported [9, 20] by other researchers and is conducive to obtaining excellent electrical properties.

3.2 Microstructure of ceramic samples

The SEM images of BCZT-Li$_x$Y$_x$ ceramic samples are shown in Fig. 3a–e and the insets of each picture are used to display the grain size distribution. It can be found that the samples of Li and Y co-doping are with bigger grain size than the pure BCZT sample. The average grain sizes of all ceramic samples are shown in Fig. 3f. In addition, it can also be seen from Fig. 3a–e that the number of intergranular pores significantly decreased due to the co-doping of Li and Y. To further verify this, the actual density of ceramic samples was measured by the Archimedes method and the relative density of ceramic samples was calculated based on the theoretical density (5.687 g/

cm^3) [13]. The density results are shown in Fig. 4. As shown in Figs. 3f and 4, the change of average grain sizes, actual density, and relative densities are consistent, which first increases and then decreases with the introduction of Li/Y. When $x = 0.3$ mol%, the average grain size, actual density, and relative density of BCZT-Li$_x$Y$_x$ ceramic samples reach the maximum value of 16.71 μm, 5.5416 g/cm^3, and 97%, respectively. This phenomenon could be explained reasonably by the following two points. On the one hand, the proper formation of oxygen vacancies due to co-doping Li/Y into BCZT ceramics can speed up the mass transfer process, which is partially responsible for grain growth and densification [11]. On the other hand, the liquid phase will appear in the sintering process due to the low melting point of Li$_2$CO$_3$ (723 °C), which can reduce the sintering temperature and promote grain growth and densification [12].

The element distribution of BCZT-Li$_x$Y$_x$ ceramic samples is displayed in Fig. 5. Although lithium cannot be detected due to the limitation of detection equipment, it can be seen that other chemical elements are homogeneously distributed in ceramic samples. Besides, there are some abnormal grains in the areas of the yellow circle in Fig. 5a, b, and e. The distribution of elements corresponding to these areas is not observed, which may be caused by the attachment of pollutants to ceramic samples.
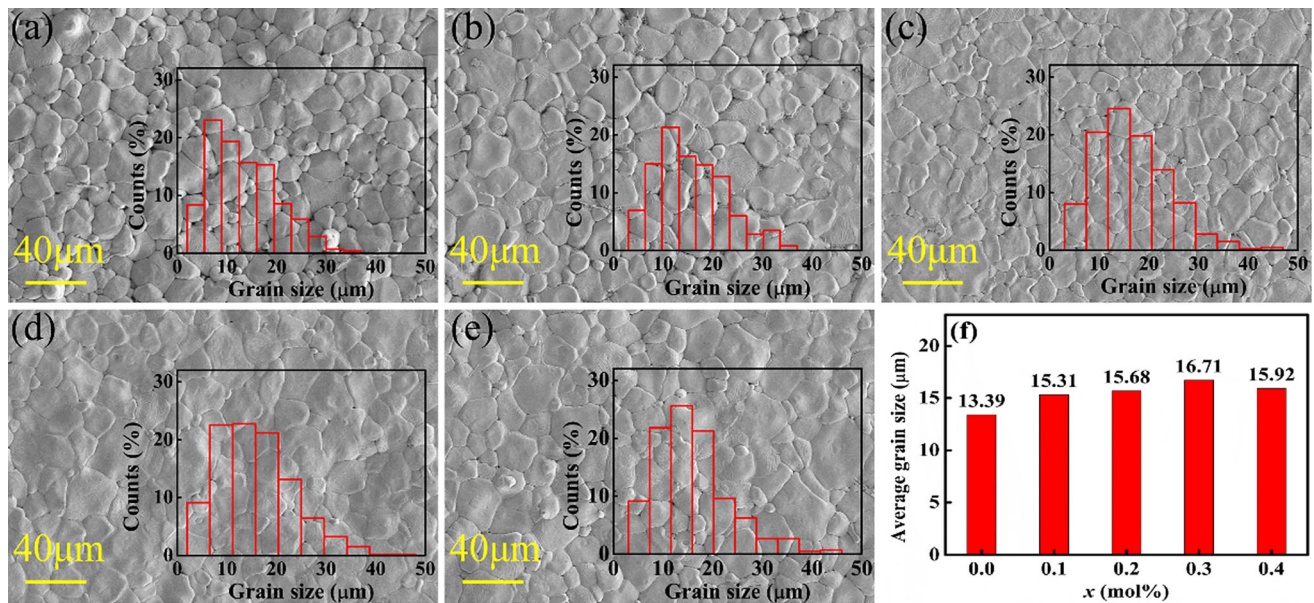
Fig. 3 SEM surface images of BCZT-Li$_x$Y$_x$. Insets exhibit grain size distribution of each composition. **a** x = 0.0 mol%, **b** x = 0.1 mol%, **c** x = 0.2 mol%, **d** x = 0.3 mol%, **e** x = 0.4 mol%. **f** the change of average grain size of ceramic samples with different doping amount of Li/Y
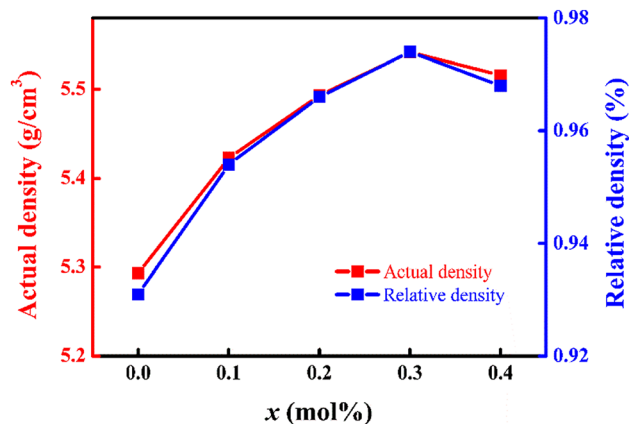

Fig. 4 Actual density and relative density of BCZT-Li$_x$Y$_x$ ceramics

3.3 Electrical properties of ceramic samples

Figure 6a exhibits the polarization–electric field loops (P–E) of BCZT-Li$_x$Y$_x$ ceramic samples, which were measured at 3 kV, 10 Hz, and room temperature. As shown in Fig. 6b, the coercive field (E_c) and remnant polarization (P_r) change with the introduction of Li/Y. It can be observed that P_r reaches the maximum at x = 0.3 mol%. This phenomenon could be explained by the following points. Firstly, the free energies of

the R–T two coexistence systems are the same. Thus, the spontaneous polarization could be easily switched along all the possible directions provided by two phases [16], which leads to the increase of P_r. Secondly, large grain size is conducive to the rotation of domain walls and high density is beneficial to obtain high dipole polarization, which can enhance the ferroelectric properties [11]. In addition, it can also be seen that the P_r value decreases at x = 0.4 mol%. The reason is that Li$^+$ ions substitute the Zr^{4+}/Ti^{4+} at B-sites will appear oxygen vacancies, which would form defect dipoles and then drag the motion of ferroelectric domain wall. This pinning effect caused the detriment of ferroelectric property at high doping content [11].

Figure 7a, b presents the change curves of piezoelectric and dielectric properties of BCZT-Li$_x$Y$_x$ ceramic samples. It can be found that the piezoelectric coefficient (d_{33}), dielectric constant (ε_r), and electromechanical coupling coefficient (k_p) have a similar variation trend, which first increases and then decreases with the addition of doping elements. The dielectric loss (tanδ) first decreases and then increases with the addition of Li/Y. In summary, the electrical properties of ceramic samples obtain an optimum level at x = 0.3 mol%, where d_{33} = 526 pC/N, k_p = 0.58%, ε_r = 4752, tanδ = 0.017, P_r = 9.73 μC/cm^2, E_c =
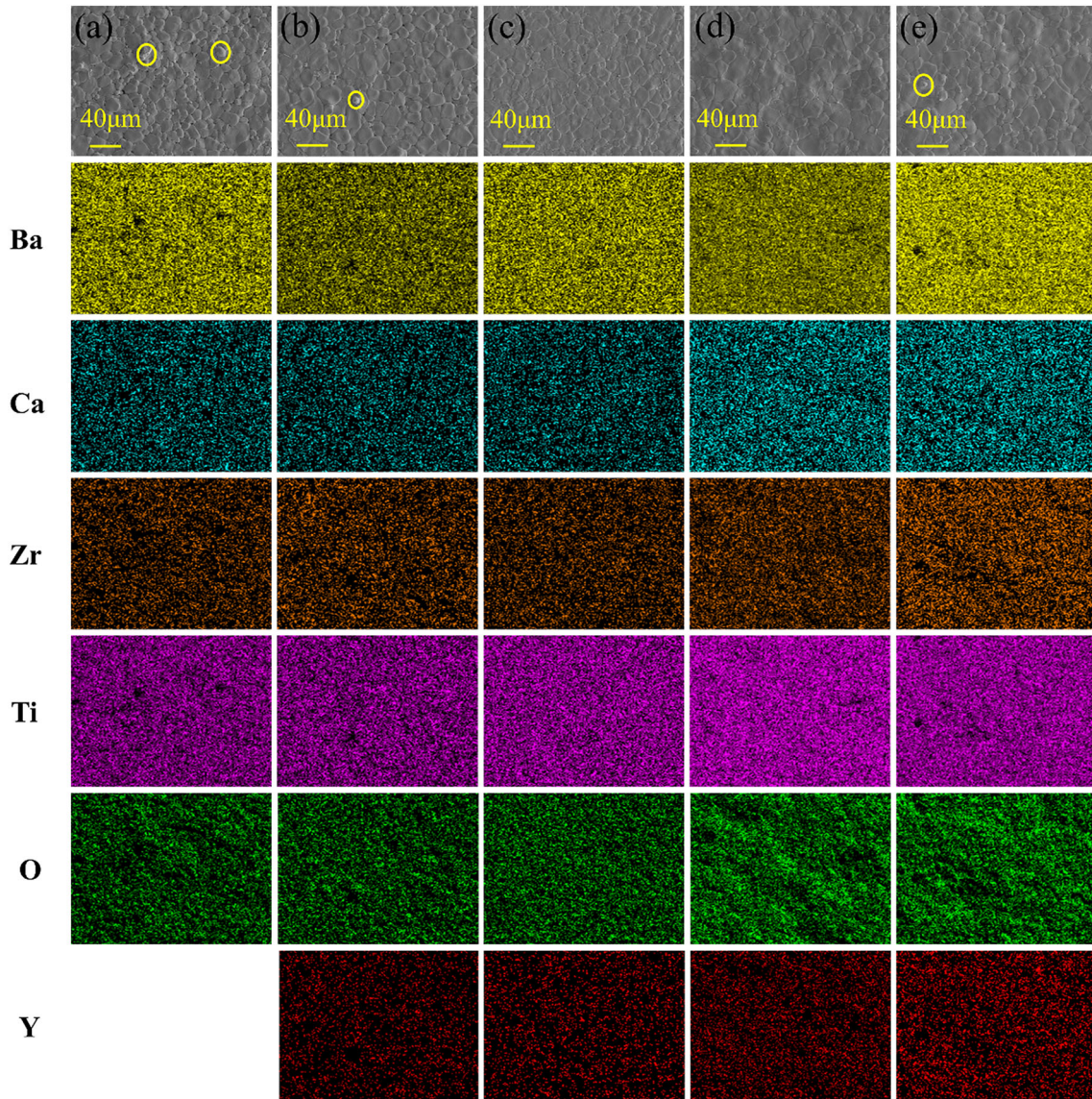
Fig. 5 Element mapping of BCZT-Li$_x$Y$_x$ ceramic samples. **a** x = 0 mol%, **b** x = 0.1 mol%, **c** x = 0.2 mol%, **d** x = 0.3 mol%, **e** x = 0.4 mol%

2.10 kV/cm. Based on the above discussion, the improvement of electrical properties is principally attributed to R–T phases coexistence, grain growth, and densification.

The piezoelectric properties of ceramics are closely related to ferroelectric and dielectric properties. Generally, the relationship between d_{33}, P_r, and ε_r can be expressed as is shown in Eq. (1) [21, 22]:

$$d_{33} = 2Q_{33r}P_r. \tag{1}$$

Here, Q_{33} represents the electrostriction coefficient, which is fixed for the same kind of material. Therefore, $\varepsilon_r P_r$ is the primary determinant of d_{33} value. As

shown in Fig. 7c, the curves of d_{33} and $\varepsilon_r P_r$ have an analogical variation trend with the change of doping contents, which indicates that the improvement of dielectric properties and ferroelectric properties is a partial reason for enhancing the piezoelectric properties of ceramic samples.

3.4 Dielectric properties of ceramic samples

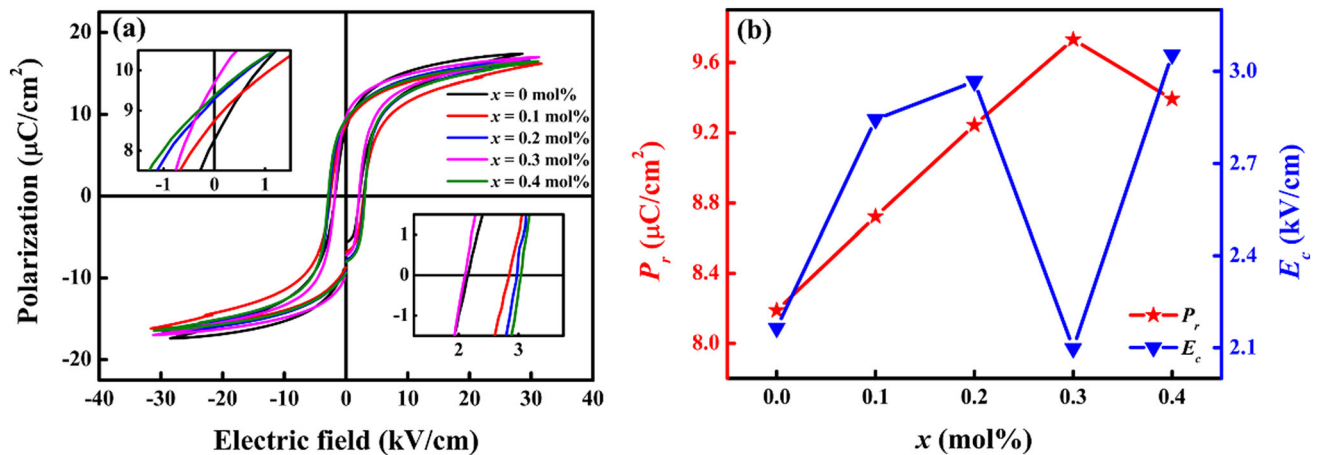Figure 8 exhibits the temperature dependence of dielectric constant of BCZT-Li$_x$Y$_x$ ceramic samples

Fig. 6 a Polarization–electric field loops (P–E) of BCZT-Li$_x$Y$_x$ ceramic samples measured at 3 kV, 10 Hz, and room temperature. Insets show a partially enlarged view of the intersection. **b** The P_r and E_c varied with x
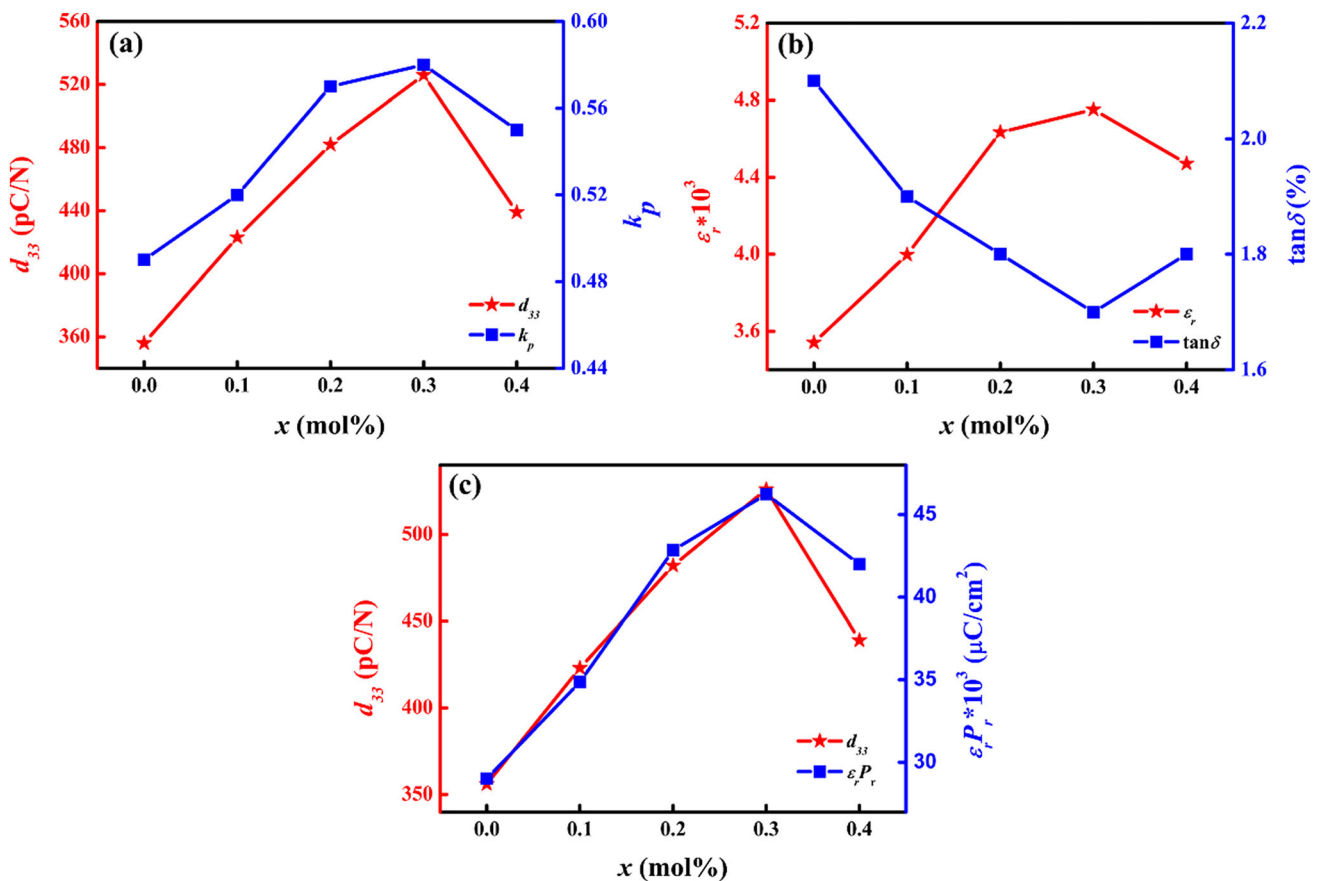

Fig. 7 a d_{33} and k_p, **b** ε_r and tanδ, **c** d_{33} and $\varepsilon_r P_r$ of BCZT-Li$_x$Y$_x$ ceramic samples

under different test frequencies with a temperature range of 20–200 °C. Two obvious phase transition peaks are observed for ceramic samples with x = 0 mol% and x = 0.1 mol%. The left one corresponds to orthorhombic–tetragonal phase transition (T_OT) and the right one corresponds to tetragonal–cubic phase transition (T_c). In addition, it can be observed that the T_c changes gradually in a temperature range (broad dielectric peak), which is called diffuse phase transition. It can also be seen that the
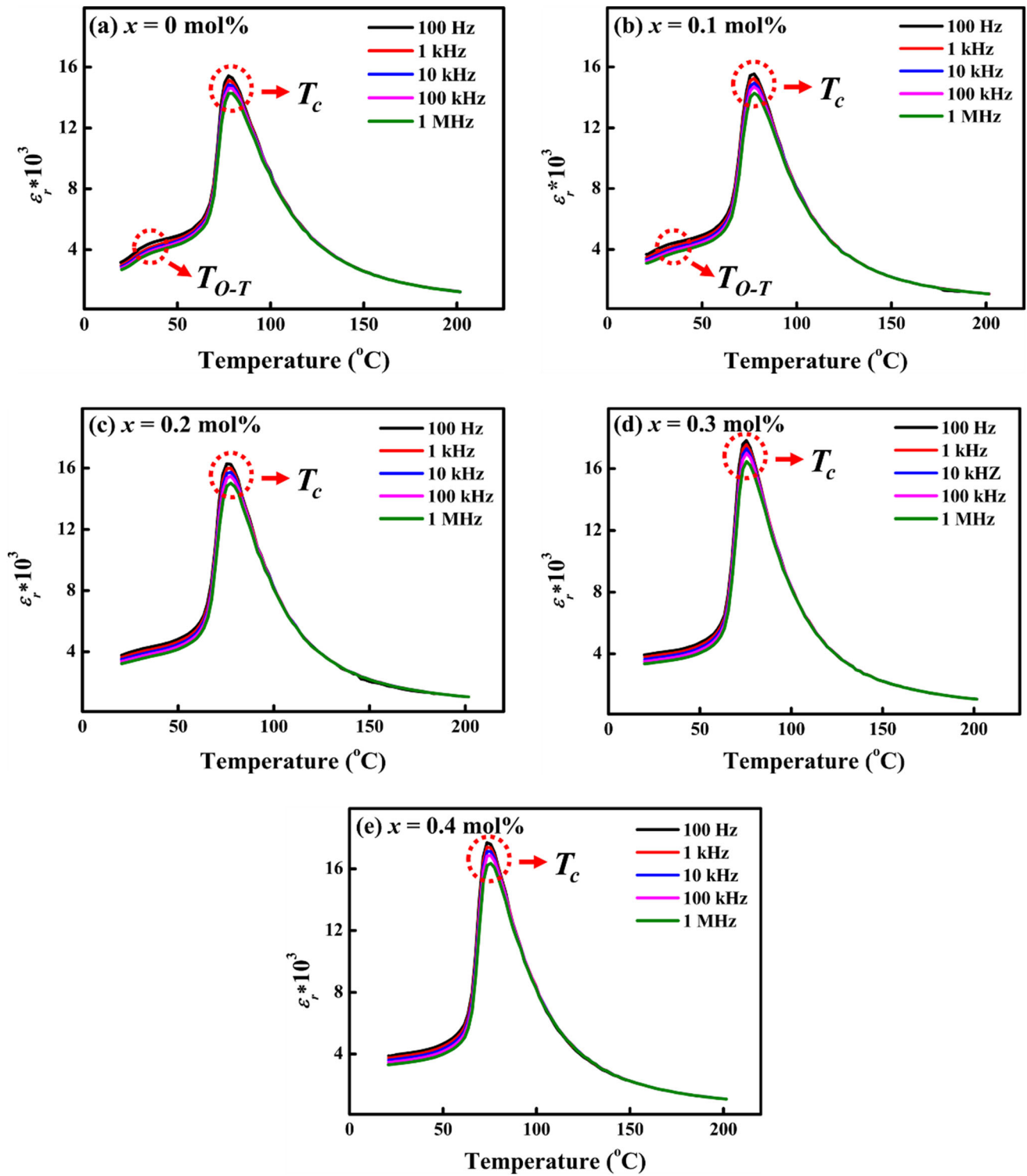
Fig. 8 Temperature dependence of dielectric constant of BCZT-Li$_x$Y$_x$ ceramic samples at various frequencies

maximum dielectric constant (ε_m) decreases as test frequency increases. This phenomenon is called frequency dispersion. Diffuse phase transition and frequency dispersion are two typical characteristics of relaxation ferroelectrics, which indicates that all ceramic samples have apparent dielectric relaxation behavior. The dielectric relaxation behavior of ceramic samples will be further studied in the next section.

Figure 9a shows the relationship between dielectric constant and temperature of BCZT-Li$_x$Y$_x$ ceramic samples. The frequency of 100 kHz is selected to avoid the influence of space charges at low frequency and high temperature. It can be seen that ε_m increases with the increase of x. The temperature corresponding to the ε_m is called Curie temperature (T_c). As shown in Fig. 9b, the change of T_c value is very small, which illustrates that the addition of Li/Y has little effect on Curie temperature of BCZT ceramics.

3.5 Dielectric relaxation behavior of ceramic samples

Figure 10 shows the reciprocal of dielectric constant as a function of temperature for BCZT-Li$_x$Y$_x$ ceramic samples at the frequency of 100 kHz. When the temperature is higher than T_c, the reciprocal of dielectric constant should follow the Curie–Weiss law of normal ferroelectrics. The function is described by Eq. (2) as follows [23]:

$$\frac{1}{\varepsilon} = \left(\frac{T - T_{cw}}{C}\right)(T > T_m). \tag{2}$$

C and T_{cw} represent the Curie–Weiss constant and the Curie–Weiss temperature, respectively. T_{cw} can be gained by fitting Eq. (2). It can be seen from Fig. 10 that the relationship between the reciprocal of dielectric constant and temperature does not conform to the Curie–Weiss law. It can be seen that these curves deviate from the Curie–Weiss law, and the degree of deviation is defined as ΔT_m in Eq. (3) [23].

$$\Delta T_m = T_B - T_m. \tag{3}$$

T_B denotes the starting temperature where the dielectric constant complies with the Curie–Weiss law. T_m represents the temperature where the dielectric constant reaches the maximum. Some parameters related to dielectric properties are listed in Table 1. The ΔT_m value first increases and then decreases with the addition of Li/Y content. The degree of diffuse phase transition is consistent with the variation trend of ΔT_m. The change of degree of diffuseness is attributed to the defect dipole and lattice distortion caused by the co-doping of Li/Y in BCZT ceramics [17, 24]. Besides, the value of ΔT_m reaches the maximum at $x = 0.3$ mol%, which means the dielectric relaxation behavior of the ceramic samples attained its maximum.

For the relaxation ferroelectric, the reciprocal of dielectric constant and temperature conforms to the modified Curie–Weiss law as is shown in Eq. (4) [23]:
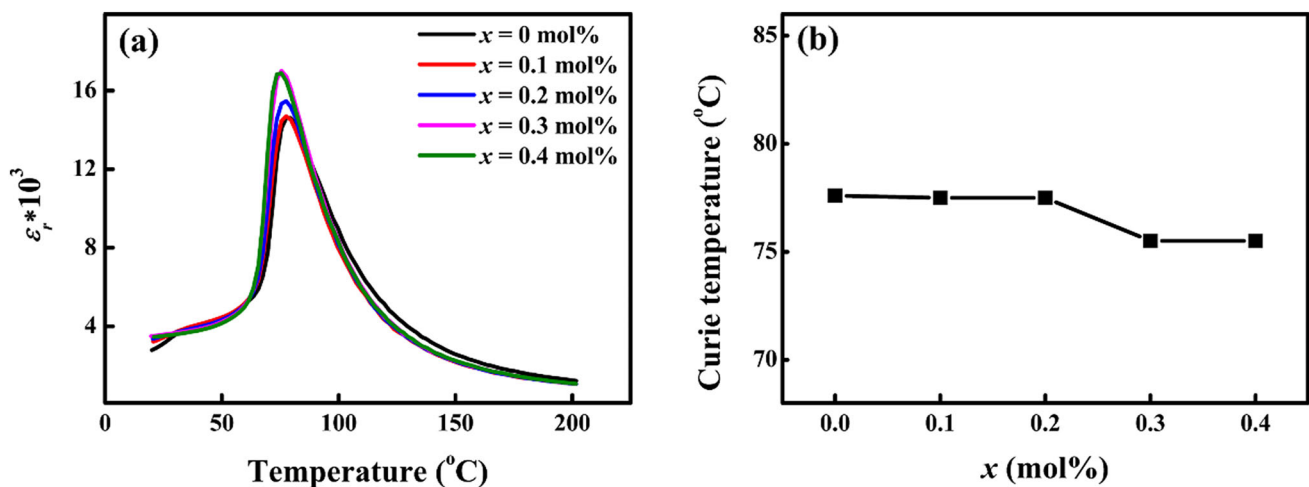

Fig. 9 **a** Temperature dependence of dielectric constant of BCZT-Li$_x$Y$_x$ ceramics at 100 kHz, **b** Curie temperature varied with x
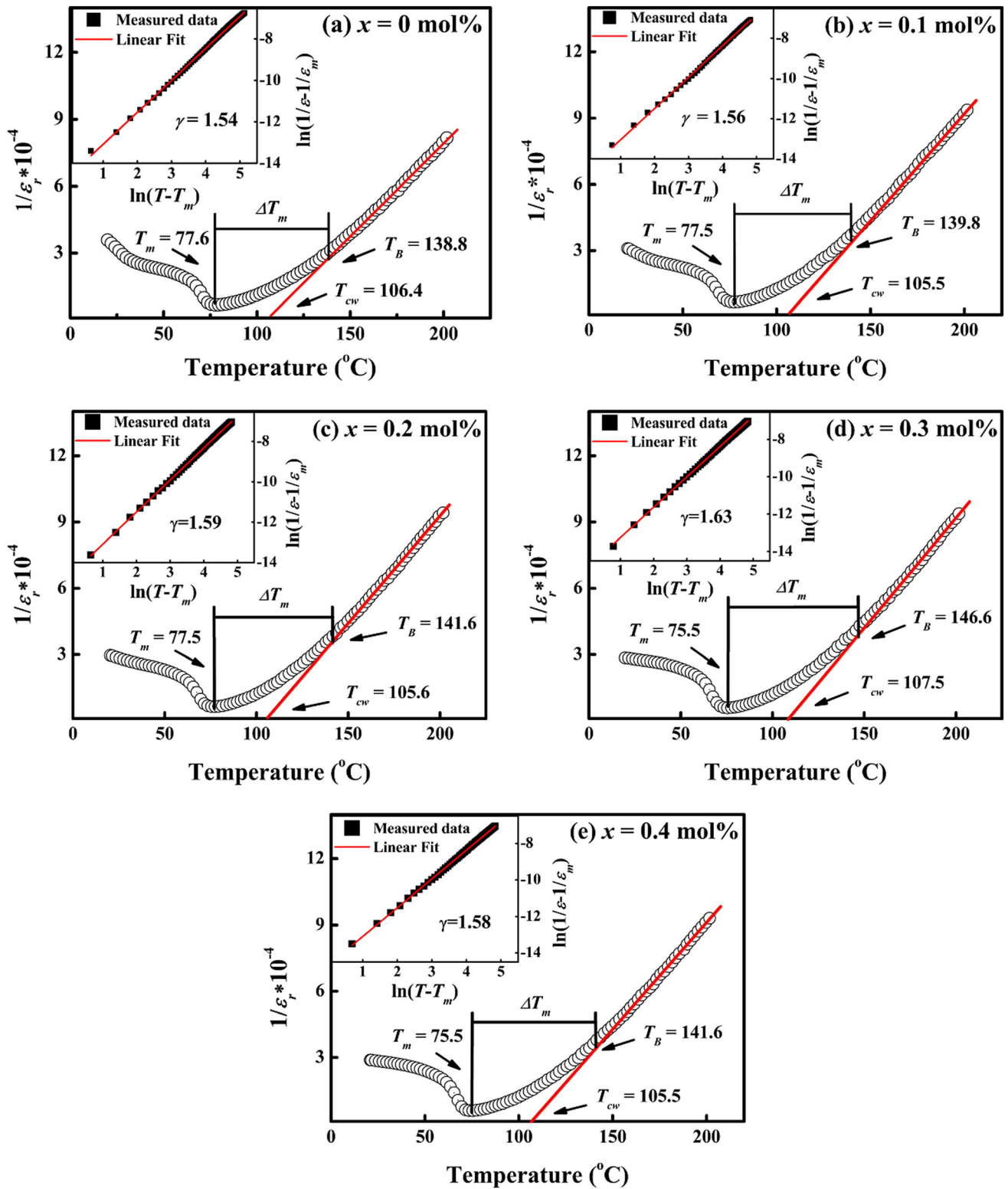
Fig. 10 The inverse dielectric constant at 100 kHz as a function of temperature for the BCZT-Li$_x$Y$_x$ ceramic samples. Insets are corresponding curves of ln(1/ε−1/ε$_m$)/ln(T−T$_m$) at 100 kHz

Table 1 Summary of some parameters extracted from dielectric measurements at 100 kHz

x (mol%)	T_{cw} (°C)	T_B (°C)	T_m (°C)	ΔT_m (°C)	ε_m (100 kHz)	γ
0	106.4	138.8	77.6	61.2	14,633	1.54
0.1	105.5	139.8	77.5	62.3	15,005	1.56
0.2	105.6	141.6	77.5	64.1	15,478	1.59
0.3	107.5	146.6	75.5	71.1	17,006	1.63
0.4	105.5	141.6	75.5	66.1	16,877	1.58

$$\frac{1}{\varepsilon} - \frac{1}{m} = \frac{(T - T_m)^{\gamma}}{C} \quad (T > T_m, 1 \le \gamma \le 2). \qquad (4)$$

Here, ε_m is the maximum dielectric constant, T_m corresponds to the temperature at which the dielectric constant reaches the maximum value, C is the Curie constant, γ represents the diffuse coefficient and its value range is greater than or equal to 1 and less than or equal to 2. When $\gamma = 1$ and $\gamma = 2$, it is suggested that the ceramic samples are normal ferroelectric and complete relaxation ferroelectric, respectively. Therefore, $1 < \gamma < 2$ indicates that the ceramic samples are relaxation ferroelectric. The value of γ can be defined by the slope of the fitted curve in the insets of Fig. 10, which is ln $(1/\varepsilon - 1/\varepsilon_m)$ as a function of ln$(T - T_m)$ at 100 kHz. The larger the γ value is in the range of 1–2, it indicates that the phase transition temperature of each micro-region is wider, and the diffuse phase transition is stronger. It can be seen from Table 1 and the insets of Fig. 10 that γ first increases and then decreases with the addition of x. Meanwhile, the values of γ reach maximum at $x = 0.3$ mol%, which indicates the dielectric relaxation behavior of the ceramic samples is the strongest.

The reason for dielectric relaxation behavior in relaxation ferroelectric can be explained by many theories [25, 26], for example, the composition fluctuations theory, the random field theory, and the merging of micropolar regions into micropolar regions. The common feature of these theories is based on the local distortion of crystal structure, resulting in polar nanoregions (PNRs). According to the principle of ionic radius similarity, Y^{3+} can replace the A-site and B-site, and Li^+ can replace the B-site in BCZT ceramics. The radius and valence of Li^+ and Y^{3+} are different from the A-site ion and the B-site ion of BCZT ceramics. The lattice distortion and charge imbalance will occur in the perovskite lattice due to the introduction of Li/Y. Hence, the PNRs will form in ceramic samples, which promotes the dielectric relaxation behavior. Besides, Li^+

occupying B-site could promote both single- and double-ionized oxygen vacancies, where single-ionized oxygen vacancies are responsible for dielectric relaxation caused by short-range hopping of oxygen vacancies [27, 28]. It can be observed that the variation trend of ΔT_m and γ is consistent and reaches maximum values of 71.1 and 1.59 at $x = 0.3$ mol%, respectively. At the same time, other electrical properties also reach the maximum at $x = 0.3$ mol%. It can be concluded that BCZT-Li$_x$Y$_x$ ceramic samples with stronger dielectric relaxation behavior have better electrical properties.

4 Conclusions

In conclusion, the BCZT-Li$_x$Y$_x$ ceramic samples were synthesized by the traditional solid-state sintering method. The effects of introducing Li/ Y into BCZT on phase structure, microstructure, and electrical properties were systematically analyzed. The XRD spectrums indicate that BCZT-LixY$_x$ ceramic samples have the perovskite structure. Rietveld refinement results show that the phase fraction of R and T is 74.8% and 25.2% at $x = 0.3$ mol%. The SEM images show that the co-doping of Li/Y in BCZT ceramics can promote grain growth and densification due to the formation of the oxygen vacancy and liquid phase. The temperature-dependent dielectric performance testing results show that ceramic samples have obvious dielectric relaxation behavior. In addition, the co-doping of Li/Y in BCZT ceramics can significantly reduce the sintering temperature from 1540 °C to 1400 °C owing to the formation of liquid phase sintering and improve the electrical properties due to the factors such as R–T phases coexistence, grain growth, and densification. The ceramic samples obtain the optimal electrical properties at $x = 0.3$ mol%, where $d_{33} = 526$ pC/N, $k_p = 58\%$, $\varepsilon_r = 4724$,

$\tan\delta = 0.017$, T_c=75.5 °C, $\gamma = 1.63$, $P_r = 9.73$ $\mu C/cm^2$, $E_c = 2.10$ kV/cm.

Acknowledgements

Author contributions

All authors have approved the final version of the manuscript.

Declarations

Conflict of interest The author declares that they have no conflict of interest.

References

1. J. Rödel, W. Jo, K.T.P. Seifeert, E.M. Anton, T. Granzow, Perspective on the development of lead-free piezoceramics. J. Am. Ceram. Soc. **92**(6), 1153–1177 (2009)

2. J. Rödel, K.G. Webber, R. Dittmer, W. Jo, M. Kimura, D. Damjanovic, Transferring lead-free piezoelectric ceramics into application. J. Eur Ceram. Soc. **35**(6), 1659–1681 (2015)

3. B. Wu, H.J. Wu, J.G. Wu, D.Q. Xiao, J.G. Zhu, S.J. Pennycook, Giant piezoelectricity and high Curie temperature in nanostructured alkali niobate lead-free piezoceramics through phase coexistence. J. Am. Chem. Soc. **138**(47), 15459–15464 (2016)

4. P.K. Panda, B. Sahoo, PZT to lead free piezo ceramics: a review. Ferroelectrics **474**(1), 128–143 (2015)

5. T. Zheng, J.G. Wu, D.Q. Xiao, J.G. Zhu, Recent development in lead-free perovskite piezoelectric bulk materials. Prog. Mater. Sci. **98**, 552–624 (2018)

6. P.K. Panda, Review: environmental friendly lead-free piezoelectric materials. J. Mater. Sci. **44**(19), 5049–5062 (2009)

7. M. Acosta, N. Novak, V. Rojas, S. Patel, R. Vaish, $BaTiO_3$-based piezoelectrics: fundamentals, current status, and perspectives. Appl. Phys. Rev. **4**(4), 041305 (2017)

8. Y. Zhang, H.J. Sun, W. Chen, A brief review of $Ba(Ti_{0.8}Zr_{0.2})O_3$-$(Ba_{0.7}Ca_{0.3})TiO_3$ based lead-free piezoelectric ceramics: past, present and future perspectives. J. Phys. Chem. Solids **114**, 207–219 (2018)

9. W.F. Liu, X.B. Ren, Large piezoelectric effect in Pb-free ceramics. Phys. Rev. Lett. **103**(25), 257602 (2009)

10. P. Wang, X.Y. Li, Y.Q. Lu, Enhanced piezoelectric properties of $(Ba_{0.85}Ca_{0.15})(Ti_{0.9}Zr_{0.1})O_3$ lead-free ceramics by optimizing calcination and sintering temperature. J. Eur. Ceram. Soc. **31**(11), 2005–2012 (2011)

11. Y. Zhang, H.J. Sun, W. Chen, Li-modified $Ba_{0.99}Ca_{0.01}Zr_{0.02}Ti_{0.98}O_3$ lead-free ceramics with highly improved piezoelectricity. J. Alloys Compd. **694**, 745–751 (2017)

12. X.M. Chen, X.Z. Ruan, K.Y. Zhao, X.Q. He, J.T. Zeng, Y.S. Li, L.Y. Zheng, C.H. Park, G.R. Li, Low sintering temperature and high piezoelectric properties of Li-doped $(Ba,Ca)(Ti,Zr)O_3$ lead-free ceramics. J. Alloys Compd. **632**, 103–109 (2015)

13. X.M. Chen, J.T. Zeng, D. Kim, L.Y. Zheng, Q.W. Lou, C.H. Park, G.R. Li, Understanding of role of Li in high-performance Pb-free Li-doped $(Ba_{0.85}Ca_{0.15})(Ti_{0.9}Zr_{0.1})O_3$ piezoceramics from theory and experiments. Mater. Chem. Phys. **231**, 173–180 (2019)

14. Y.C. Lee, Y.L. Huang, Effects of CuO doping on the microstructural and dielectric properties of $Ba_{0.6}Sr_{0.4}TiO_3$ ceramics. J. Am. Ceram. Soc. **92**(11), 2661–2667 (2009)

15. Z.M. Wang, X.F. Chen, X.L. Chao, J.J. Wang, P.F. Liang, Z.P. Yang, Low temperature sintering and dielectric properties of $(Ba_{0.85}Ca_{0.15})(Ti_{0.9}Zr_{0.1})O_3$-$xCu^{2+}$ ceramics obtained by the sol-gel technique. Ceram. Int. **42**(16), 18037–18044 (2016)

16. S. Mittal, R. Laishram, K.C. Singh, Multi-phase coexistence in yttrium-substituted $Ba_{0.9}Ca_{0.1}Zr_{0.07}Ti_{0.93}O_3$ lead-free piezoceramics. Ceram. Int. **45**(1), 1237–1245 (2019)

17. Y.H. Wu, F. Ma, J.K. Qu, Y. Luo, J. Song, G.Y. Wei, Y.C. Zhang, T. Qi, Role of Cu and Y in sintering, phase transition, and electrical properties of BCZT lead-free piezoceramics. Ceram. Int. **44**(13), 15001–15009 (2018)

18. L.F. Zhu, B.P. Zhang, L. Zhao, J.F. Li, High piezoelectricity of $BaTiO_3$–$CaTiO_3$–$BaSnO_3$ lead-free ceramics. J. Mater. Chem. C **2**(24), 4764–4771 (2014)

19. T. Yang, X.H. Ke, Y.Z. Wang, Mechanisms responsible for the large piezoelectricity at the tetragonal-orthorhombic phase boundary of $(1-x)BaZr_{0.2}Ti_{0.8}O3$-$xBa_{0.7}Ca_{0.3}TiO_3$ system. Sci. Rep. **6**, 33392 (2016)

20. X. Liu, Z.H. Chen, B.J. Fang, J.N. Ding, X.Y. Zhao, H.Q. Xu, H.S. Luo, Enhancing piezoelectric properties of BCZT ceramics by Sr and Sn co-doping. J. Alloys Compd. **640**, 128–133 (2015)

21. Q.W. Zhang, H.Q. Sun, X.S. Wang, Y. Zhang, X. Li, Strong photoluminescence and piezoelectricity properties in Pr-doped $Ba(Zr_{0.2}Ti_{0.8})O_3$–$(Ba_{0.7}Ca_{0.3})TiO_3$ ceramics: influence

of concentration and microstructure. J. Eur. Ceram. Soc. **34**(5), 1439–1444 (2014)

22. Y.S. Tian, Y.Y.S. Gong, D.W. Meng, Y.J. Li, B.Y. Kuang, Dielectric dispersion, diffuse phase transition, and electrical properties of BCT–BZT ceramics sintered at a low-temperature. J. Electron. Mater. **44**(8), 2890–2897 (2015)

23. E.P. Cai, Q.B. Liu, F.F. Zeng, Y.Y. Wang, A. Xue, A comparative study of lead-free $(Ba_{0.85}Ca_{0.15})(Ti_{0.9}Zr_{0.08}Sn_{0.02})O_3$ ceramics prepared by conventional sintering and microwave sintering techniques. Ceram. Int. **44**(1), 788–798 (2018)

24. P. Jaiban, P. Wannasut, P. Kantha, M. Promsawat, A. Watcharapasorn, Effects of Mg and La co-doping on dielectric, ferroelectric, and piezoelectric properties of barium calcium zirconate titanate ceramics. Chiang Mai J. Sci. **47**(4), 633–641 (2020)

25. I.W. Chen, Structural origin of relaxor ferroelectrics—revisited. J. Phys. Chem. Solids. **61**(2), 197–208 (2000)

26. A.A. Bokov, Z.G. Ye, Recent progress in relaxor ferroelectrics with perovskite structure. J. Mater. Sci. **41**(1), 31–52 (2006)

27. A. Limpichaipanit, A. Ngamjarurojana, Effect of Li and Bi co-doping and sintering temperature on dielectric properties of PLZT 9/65/35 ceramics. Ceram. Int. **43**(5), 4450–4455 (2017)

28. X.F. Wang, P.F. Liang, L.L. Wei, X.L. Chao, Z.P. Yang, Diffusion phase transition and impedance spectroscopy of Bi_2O_3/CuO co-doped BCZT lead-free ceramics. J. Mater. Sci.: Mater. Electron. **27**(4), 3217–3226 (2016)

Publisher's Note Springer Nature remains neutral with regard to jurisdictional claims in published maps and institutional affiliations.